



Capture of gaseous elemental mercury from flue gas using a magnetic and sulfur poisoning resistant sorbent Mn/ γ -Fe₂O₃ at lower temperatures

Shijian Yang, Yongfu Guo, Naiqiang Yan*, Zan Qu, Jiangkun Xie, Chen Yang, Jinping Jia

School of Environmental Science and Engineering, Shanghai Jiao Tong University, 800 Dong Chuan Road, Shanghai, 200240, PR China

ARTICLE INFO

Article history:

Received 8 September 2010
Received in revised form 6 November 2010
Accepted 8 November 2010
Available online 13 November 2010

Keywords:

Magnetic sorbent
Capture capacity
Elemental mercury
SO₂ poisoning

ABSTRACT

A series of Mn/ γ -Fe₂O₃ were synthesized to capture elemental mercury from the flue gas. Mn⁴⁺ cations and cation vacancies on the surface played important roles on elemental mercury capture by Mn/ γ -Fe₂O₃. Furthermore, the reaction route of elemental mercury oxidation was dependent on the ratio of Mn⁴⁺ cations to cation vacancies. As a result, the capacities of 15%-Mn/ γ -Fe₂O₃-250 for elemental mercury capture were generally higher than those of 30%-Mn/ γ -Fe₂O₃-400. SO₂ mainly reacted with \equiv Fe^{III}-OH and only a small amount of \equiv Mn⁴⁺ reacted with SO₂, so the presence of a high concentration of SO₂ resulted in an insignificant effect on elemental mercury capture by 15%-Mn/ γ -Fe₂O₃-250 at lower temperatures. The capacities of 15%-Mn/ γ -Fe₂O₃-250 for elemental mercury capture in the presence of 2.8 g N m⁻³ of SO₂ were more than 2.2 mg g⁻¹ at <200 °C. Meanwhile, 15%-Mn/ γ -Fe₂O₃-250 can be separated from the fly ash using magnetic separation, leaving the fly ash essentially free of sorbent and adsorbed HgO. Therefore, 15% Mn/ γ -Fe₂O₃-250 may be a promising sorbent for elemental mercury capture.

© 2010 Elsevier B.V. All rights reserved.

1. Introduction

The emission of mercury from anthropogenic activities is a serious concern in both developed and developing countries [1]. Coal-fired utility boilers are currently the largest single-known source of anthropogenic mercury emissions. In the United States, about one-third of the 150 tons of mercury emitted comes from coal-fired utility boiler [2]. In China, about 38% of the emission of mercury comes from coal combustion [3]. In addition to particulate-bound mercury (Hg^p), both elemental mercury (Hg⁰) and oxidized mercury (Hg²⁺) are present as the gaseous mercury species in the flue gas from coal-fired utilities [4]. Particulate-bound mercury and oxidized mercury (mainly HgCl₂) can be effectively removed from the plant effluent by particulate control devices and wet scrubbing or SO₂ control devices, respectively [5]. Gaseous elemental mercury is difficult to be removed using currently available removal devices due to its unsolvability in water [6]. Therefore, elemental mercury is the major mercury species emitted in the stack flue gas from coal-fired utilities [7].

Catalysts/sorbents for elemental mercury removal studied to date mainly fall into one of three groups: carbon-based sorbents, selective catalytic reduction catalysts, and metals and metal oxides [2]. The oxidants likely involved are mainly chlorine and oxygen.

* Corresponding author. Tel.: +86 21 54745591.

E-mail addresses: yangshijiangsq@163.com (S. Yang), nqyan@sjtu.edu.cn (N. Yan).

For the oxidization of elemental mercury by chlorine, there is a correlation between HCl concentration in the flue gas and the extent of elemental mercury oxidization [2]. In China, the content of chlorine in the feed-coal (63–318 mg kg⁻¹) is much lower than the average value of US coals (628 mg kg⁻¹) [8], so oxidizing elemental mercury using gaseous oxygen in the flue gas is an economical method for the control of elemental mercury emission. Furthermore, the oxidized mercury formed (HgO or Hg₂O) adsorbs to the catalyst/sorbent, and is then removed from the flue gas. Now, the mercury-sorbent materials are extremely restricted in the application for at least four reasons: sorbent recovery, removal of toxin from the industrial waste [9], interference of the chemical composition in the flue gas and cost of operation. First, the spent sorbent for elemental mercury capture is generally collected together with the fly ash particulate by particulate control devices such as fabric filters or electrostatic precipitators [9]. It will be difficult and impractical to reclaim the spent sorbent from the fly ash mixture for regeneration. Second, the fly ash will be contaminated by the mercury adsorbed on the sorbent if the spent sorbent is not effectively removed from the fly ash. If the contaminated fly ash is used as a cement additive, the toxin may release in the cement plant during the calcination process. Third, the chemical composition in the flue gas (especially SO₂ or SO₃) significantly affects elemental mercury capture by sorbents [10–13]. SO₂ molecules may compete with gaseous elemental mercury for the activity sites. The concentration of SO₂ in the real flue gas is about 10⁴–10⁵ times that of elemental mercury (v/v) [12,13]. Furthermore, SO₂ can react with metals and metal oxides to form a surface sulfate species [14,15],

which may make them inefficient for elemental mercury capture. Fourth and mostly importantly, the sorbent must be cheap and easy to operate.

The separation of the sorbent containing mercury from the fly ash can be solved by the magnetic property of sorbent material [16,17]. A magnetic sorbent MagZ–Ag⁰ has been investigated for elemental mercury capture [9,18], but more cost-effective sorbents should be developed. In our previous research, a cheap magnetic sorbent (Fe₂Ti)_{0.8}O₄ was used for elemental mercury capture. However, the presence of a high concentration of SO₂ resulted in an obvious interference with elemental mercury capture.

Herein, a series of Mn/γ-Fe₂O₃ were synthesized and characterized using X-ray diffraction (XRD), N₂ adsorption/desorption isotherm, X-ray photoelectron spectroscopy (XPS) and magnetization measurement. Then, a packed-bed reactor system was used to estimate their performance for elemental mercury capture.

2. Experimental

2.1. Samples preparation

A mixture containing 0.15 mol L⁻¹ of ferrous sulfate and 0.15 mol L⁻¹ of ferric trichloride (200 mL) was added into an ammonia solution (100 mL), leading to an instantaneous precipitation of nanosized magnetite. After stirring for 2 h, 100 mL of manganous sulfate solution (0.10 or 0.30 mol L⁻¹) was added into the suspension. During the preparation, the system was continuously stirred at 800 rpm. The particles were separated by centrifugation at 4500 rpm for 5 min and washed with distilled water followed by a new centrifugation. After 3 washings, the particles were collected and dried in a vacuum oven at 105 °C for 12 h. Mn/γ-Fe₂O₃-250 and -400 were obtained after the thermal treatment at 250 °C and 400 °C under air for 3 h, respectively. The mole ratios of Fe to Mn in 15%-Mn/γ-Fe₂O₃ and 30%-Mn/γ-Fe₂O₃ were about 6 and 2, respectively.

2.2. Sorbent characterization

Powder X-ray diffraction pattern was recorded between 20° and 70° at a step of 2° min⁻¹ on an X-ray diffractometer (Rigaku, D/max-2200/PC) with Cu Kα radiation (30 kV and 30 mA). BET Surface area was determined by the BET method using N₂ adsorption–desorption isotherm. N₂ adsorption–desorption isotherm was measured on a gas sorption analyzer (Micromeritics, ASAP 2010 M+C) at a liquid nitrogen temperature. Prior to measurement, samples were outgassed at 200 °C for 2 h. Saturation magnetization was determined using a vibrating sample magnetometer (VSM, Model JDM-13) at room temperature. XPS (Thermo ESCALAB 250) with Al Kα (*hν* = 1486.6 eV) as the excitation source was used to determine the binding energies of Fe 2p, Mn 2p, O 1s, S 2p and Hg 4f. The C 1s line at 284.6 eV was taken as a reference for the binding energy calibration.

2.3. Elemental mercury capture

The assembly used for elemental mercury capture was similar to that previously described by Granite et al. [19]. It consisted of an elemental mercury permeation tube, a packed-bed reactor, a cold vapor atomic absorption spectrometer (CVAAS) and an online data acquisition system. A flow of air passed through the permeation tube and yielded a stable concentration of elemental mercury. A temperature control device was employed to keep the reactor at desired temperatures. The gas containing elemental mercury first passed through the blank tube, and then entered the CVAAS to determine the baseline. When the concentration of elemental mercury had fluctuated within ±5% for more than 30 min, the gas was

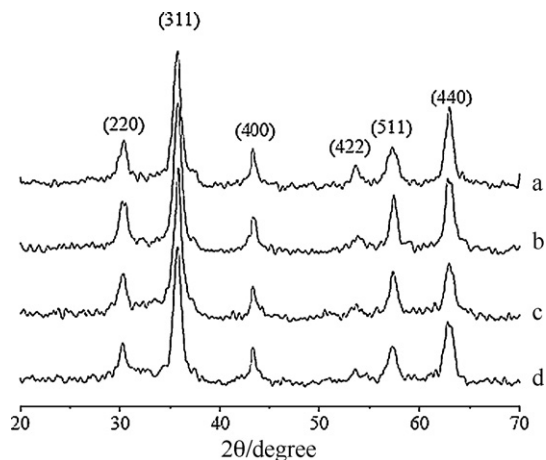


Fig. 1. XRD patterns of synthesized: (a), 15%-Mn/γ-Fe₂O₃-250; (b), 15%-Mn/γ-Fe₂O₃-400; (c), 30%-Mn/γ-Fe₂O₃-250; (d), 30%-Mn/γ-Fe₂O₃-400.

diverted to pass through the adsorbent bed for the test. The reactor was a quartz tube with an outer diameter of 8 mm and an inner diameter of 6 mm. The quartz wool was packed in the reactor tube to support the sorbent layer and avoid its loss. It was demonstrated that quartz wool has no ability for elemental mercury capture [20].

To preliminarily estimate the performance for elemental mercury capture, Mn/γ-Fe₂O₃ was first tested under air. The inlet gas contained about 1.00 mg N m⁻³ (±20%) of elemental mercury and 2% of H₂O with a feed of 12 L h⁻¹. For each test, the time was about 10 h, the sorbent mass was 30.0 mg (the gas space velocity was about 1.2 × 10⁶ h⁻¹) and the reaction temperatures varied from 100 to 300 °C.

Then, the effect of a high concentration of SO₂ on elemental mercury capture was investigated. The inlet gas contained about 1.00 mg N m⁻³ (±20%) of elemental mercury, 2.8 g N m⁻³ (1000 ppm) of SO₂, 2% of H₂O and 10% of O₂ with a feed of 12 L h⁻¹.

The concentration of elemental mercury in the gas was analyzed using an SG-921 CVAAS. Meanwhile, the concentration of Hg²⁺ at the exit of reactor was determined using the Ontario Hydro Method [8]. The breakthrough curve was generated by plotting the CVAAS voltage signal.

3. Results and discussion

3.1. Sorbent characterization

3.1.1. XRD

XRD patterns of synthesized samples are shown in Fig. 1. The characteristic reflections corresponded very well to the standard card of maghemite (JCPDS: 39-1346). Additional reflections that would indicate the presence of any crystalline manganese oxides, such as Mn₃O₄ (hausmannite), Mn₂O₃ (bixbyite) or MnO₂, were not present in the diffraction scan. The lattice parameters of synthesized samples were all about 0.834 nm, which were approximately equal to that of pure maghemite. It indicates that Mn cation was present as an amorphous phase of MnO_x and few Mn cations were incorporated into the structure of γ-Fe₂O₃. Crystal sizes of synthesized samples were calculated with the Scherrer's equation [21] (shown in Table 1).

3.1.2. XPS

Surface information on synthesized samples was analyzed by XPS. XPS spectra over the spectral regions of Fe 2p, Mn 2p and O 1s were evaluated (shown in Fig. 2). The Fe peaks were assigned to oxidized Fe species, more likely Fe³⁺ type species [22,23]. The binding energies centered at about 710.0 and 711.2 eV may be assigned

Table 1
Crystal size, magnetization and BET surface area of synthesized sample.

	Crystal size (nm)	Saturation magnetization (emu g^{-1})	BET surface area ($\text{m}^2 \text{g}^{-1}$)
15%-Mn/ γ - Fe_2O_3 -250	8.3	43.9	87.6
15%-Mn/ γ - Fe_2O_3 -400	10	45.3	83.0
30%-Mn/ γ - Fe_2O_3 -250	8.3	45.4	90.2
30%-Mn/ γ - Fe_2O_3 -400	10	42.9	77.8

to Fe^{3+} in the spinel structure, and the binding energy centered at about 712.4 eV may be ascribed to Fe^{3+} bonded with hydroxyl group. The O peaks mainly centered at about 530.0 eV, as expected for the transition metal oxides. Another oxygen species centered at about 531.1 eV was also observed, which was assigned to O in $-\text{OH}$ [22,23]. The Mn peaks were assigned to Mn^{3+} (641.2 eV) and Mn^{4+} (642.3 eV). The percents of O, Mn and Fe species on Mn/ γ - Fe_2O_3 are shown in Table 2.

3.1.3. Magnetization

A key feature of synthesized Mn/ γ - Fe_2O_3 for elemental mercury capture is its magnetic property, which makes it possible to separate the sorbent from the fly ash. The saturation magnetizations of synthesized samples were all about 40 emu g^{-1} (shown in Table 1).

Although the crystal sizes of synthesized Mn/ γ - Fe_2O_3 were all less than 10 nm (shown in Table 1), their particulate sizes were higher than $100 \mu\text{m}$ due to the agglomeration after the thermal

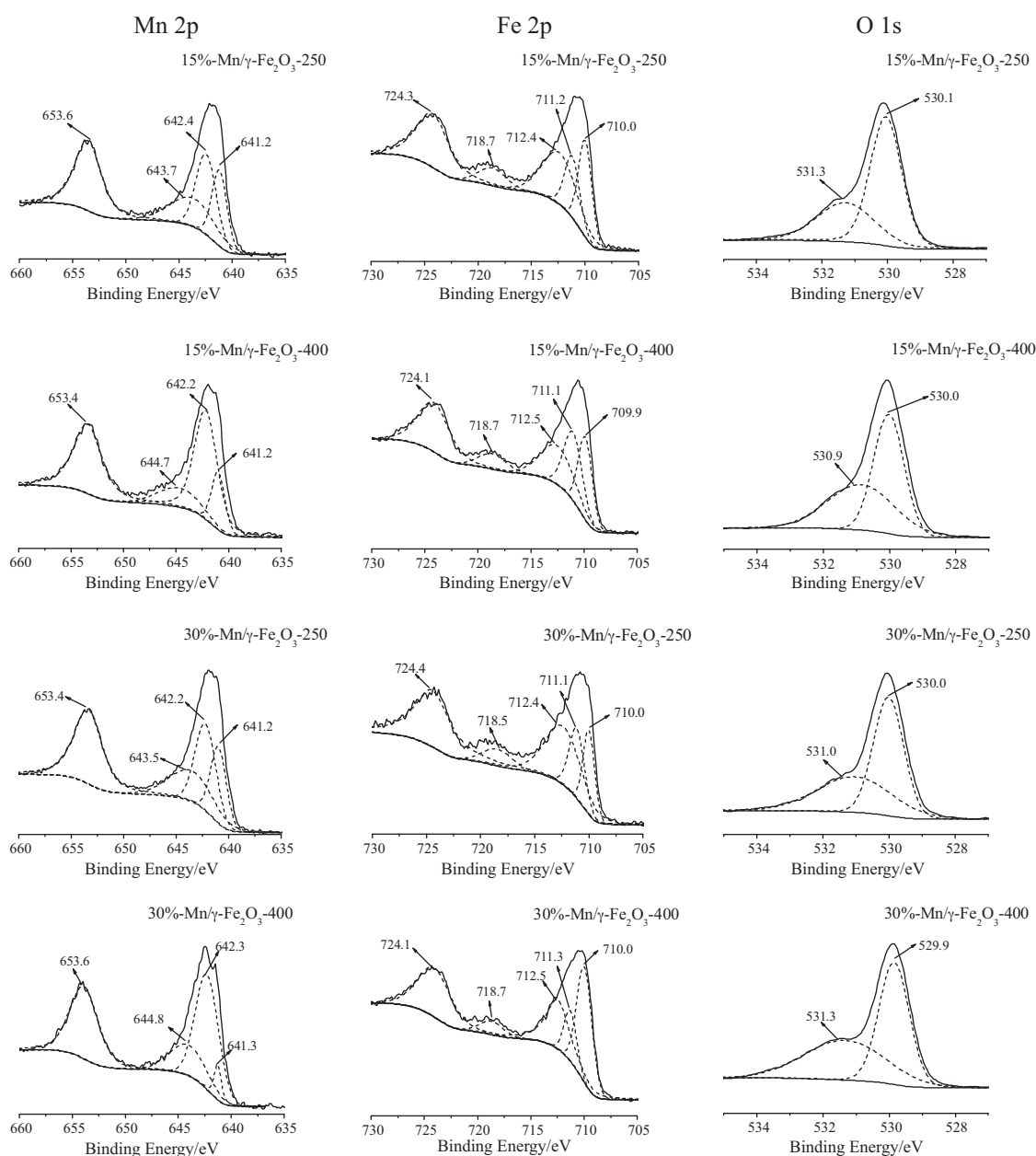
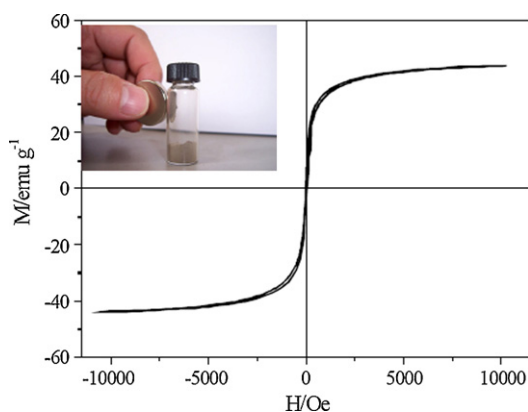


Fig. 2. XPS spectra of synthesized samples over the spectral regions of Fe 2p, Mn 2p and O 1s.

Table 2
Data of atomic ratios collected from XPS/%.

	□	O	Fe	Fe ³⁺	≡Fe ^{III} -OH	Fe-SO ₄ ²⁻	Mn	Mn ²⁺	Mn ³⁺	Mn ⁴⁺	MnSO ₄
15%-Mn/γ-Fe ₂ O ₃ -250	3.3	61.5	26.2	14.1	12.1	–	12.3	–	5.2	7.1	–
15%-Mn/γ-Fe ₂ O ₃ -400	3.4	60.3	27.5	17.6	9.9	–	12.2	–	2.7	9.5	–
30%-Mn/γ-Fe ₂ O ₃ -250	2.7	60.5	21.9	10.3	11.6	–	17.3	–	7.1	10.2	–
30%-Mn/γ-Fe ₂ O ₃ -400	2.4	65.3	19.6	11.8	7.8	–	15.1	–	1.1	14.0	–
15%-Mn/γ-Fe ₂ O ₃ -250 after test without SO ₂	–	63.0	26.1	14.4	11.7	–	10.6	2.5	3.1	5.0	–
30%-Mn/γ-Fe ₂ O ₃ -400 after test without SO ₂	–	63.6	20.5	11.5	9.0	–	15.7	–	5.8	9.9	–
15%-Mn/γ-Fe ₂ O ₃ -250 after test with SO ₂	–	66.0	24.5	14.0	5.4	5.1	7.2	2.2	2.1	2.9	–
15%-Mn/γ-Fe ₂ O ₃ -400 after test with SO ₂	–	69.7	19.6	10.4	4.3	4.9	7.1	–	1.7	3.1	2.3

**Fig. 3.** Magnetization characteristics of synthesized 15%-Mn/γ-Fe₂O₃-250.

treatment. The magnetic sorbents can first be removed from the flue gas together with the fly ash by an electrostatic precipitator, and then the magnetic sorbents and adsorbed mercury can be separated from the fly ash using magnetic separation [9,18]. The photograph inserted in Fig. 3 shows the result of separating 1 g of 15%-Mn/γ-Fe₂O₃-250 from 10 g of fly ash by a normal magnet. After 15%-Mn/γ-Fe₂O₃-250 was separated from the fly ash, the contents of Mn and Fe in the fly ash did not increase. But the mass of 15%-Mn/γ-Fe₂O₃-250 increased because some fly ash was adsorbed on it.

As shown in Fig. 3, synthesized 15%-Mn/γ-Fe₂O₃-250 showed the super-paramagnetism with a minimized coercivity and a negligible magnetization hysteresis. It ensures that 15%-Mn/γ-Fe₂O₃-250 does not become permanently magnetized after being exposed to an external magnetic field. After the external magnetic field is removed, the sorbent particles can be well re-dispersed [9].

Table 3
Capacity (Q) and breakthrough ratio (η) of synthesized Mn/γ-Fe₂O₃ for elemental mercury capture mg g⁻¹.

		100 °C	150 °C	200 °C	250 °C	300 °C
15%-Mn/γ-Fe ₂ O ₃ -250 without SO ₂	Q	2.22	2.46	3.54	2.51	2.60
	η	50%	48%	55%	56%	36%
15%-Mn/γ-Fe ₂ O ₃ -400 without SO ₂	Q	3.64	2.90	1.94	1.96	1.58
	η	19%	51%	62%	42%	81%
30%-Mn/γ-Fe ₂ O ₃ -250 without SO ₂	Q	2.70	2.28	1.62	2.14	1.68
	η	48%	61%	61%	62%	84%
30%-Mn/γ-Fe ₂ O ₃ -400 without SO ₂	Q	2.96	2.38	1.42	1.36	1.68
	η	33%	61%	68%	76%	74%
15%-Mn/γ-Fe ₂ O ₃ -250 with SO ₂	Q	2.37	2.20	3.09	1.84	1.04
	η	57%	74%	50%	75%	>90%
15%-Mn/γ-Fe ₂ O ₃ -400 with SO ₂	Q	2.11	1.60	1.08	1.59	0.52
	η	77%	83%	>90%	78%	>95%

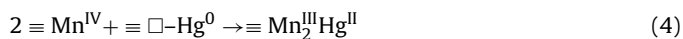
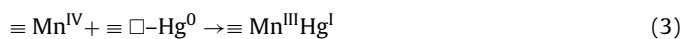
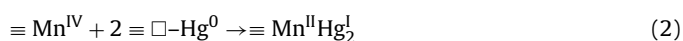
3.2. Elemental mercury capture

The determination of Hg²⁺ concentration at the exit of reactor showed that there was little Hg²⁺ in the gas after passing through the reactor tube with the magnetic sorbent. So the reduced amount of elemental mercury was captured by the magnetic sorbent. The amount of elemental mercury captured per unit mass of sorbent (capacity) can be calculated from the breakthrough curve. Table 3 shows the capacities of synthesized magnetic sorbents for elemental mercury capture (Q) and the breakthrough ratios (the ratio of the outlet concentration of elemental mercury to the inlet concentration of elemental mercury at 10 h, η) as a function of reaction temperature under air.

3.2.1. Elemental mercury capture under air

As shown in Table 3, synthesized samples all showed excellent capacities for elemental mercury capture under air (>1.5 mg g⁻¹ at 100–300 °C). The optimal reaction temperature for elemental mercury capture by 15%-Mn/γ-Fe₂O₃-250 centered at 200 °C, and those for other samples all centered at 100 °C.

Elemental mercury capture by metal oxides in the absence of halogen may be attributed to the Mars-Maessen mechanism [2,19]. The possible reactions can be described as:



Reaction (1) was the collision of elemental mercury with the surface, resulting in a physical adsorption on the cation vacancies (□). Cation vacancies were mainly on γ-Fe₂O₃ (Fe_{2.67}□_{0.33}O₄) [24]. If the concentration of elemental mercury in the gas phase

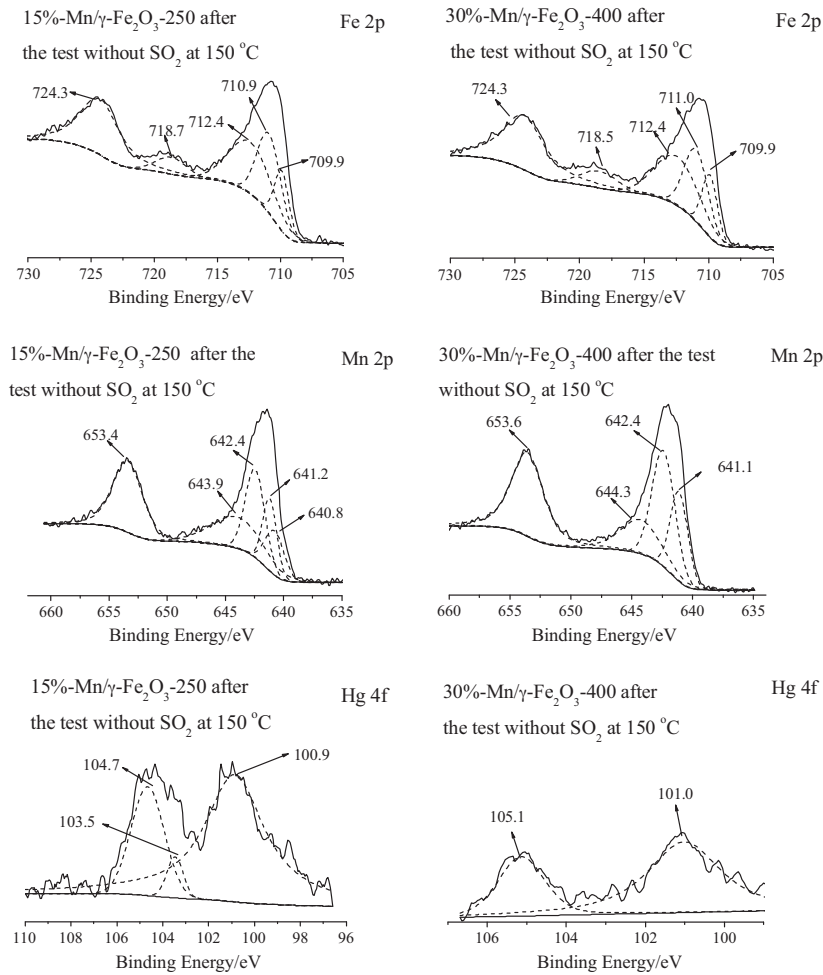


Fig. 4. XPS spectra of synthesized samples after the test without SO_2 over the spectral regions of Mn 2p, Fe 2p and Hg 4f.

was sufficiently high for the surface to be saturated with physically adsorbed elemental mercury, the concentration of physically adsorbed elemental mercury on the surface ($[\equiv \square - \text{Hg}^0]$) can be described as:

$$[\equiv \square - \text{Hg}^0] = k_1 [\equiv \square] \quad (6)$$

where $[\equiv \square]$ and k_1 were the percent of cation vacancy on the surface and the constant, respectively. Reaction (1) was an exothermic reaction, so k_1 would rapidly decrease with the increase of reaction temperature. Reactions (2)–(5) were the possible reaction routes for the oxidization of physically adsorbed elemental mercury.

The specific mechanism for elemental mercury capture by synthesized samples was studied using XPS analysis.

XPS spectra of 15%-Mn/ γ - Fe_2O_3 -250 after elemental mercury capture under air at 150°C are shown in Fig. 4. In comparison with fresh 15%-Mn/ γ - Fe_2O_3 -250 (shown in Fig. 2), no obvious changes happened over the spectral region of Fe 2p. But the percent of Mn^{4+} decreased from 7.1% to 5.0%, and a new component (640.8 eV) appeared, which may be ascribed to Mn^{2+} cations. Considering the binding energies of Hg 4f 7/2 at 100.9 eV and Hg 4f 5/2 at 104.7 eV, the oxidized mercury formed was HgO . The peak at 103.5 eV was attributed to Si 2p of SiO_2 in quartz wool. They suggest that elemental mercury capture by 15%-Mn/ γ - Fe_2O_3 -250 may mainly follow Reaction (5).

The kinetic equation of Reaction (5) can be described as:

$$\begin{aligned} -\frac{d[\equiv \text{Mn}^{\text{IV}}]}{dt} &= -\frac{d[\equiv \square - \text{Hg}^0]}{dt} = \frac{d[\equiv \text{Mn}^{\text{II}}\text{Hg}^{\text{II}}]}{dt} = k[\equiv \text{Mn}^{\text{IV}}] \\ &= [\equiv \square - \text{Hg}^0] \end{aligned} \quad (7)$$

where $[\equiv \text{Mn}^{\text{IV}}]$ and k were the percent of Mn^{4+} cation on the surface and the kinetic constant, respectively. Reaction (5) was promoted with the increase of reaction temperature, so k would increase with the increase of reaction temperature.

According to Eq. (6), Eq. (7) was transformed as:

$$\begin{aligned} -\frac{d[\equiv \square - \text{Hg}^0]}{dt} &= -\frac{k_1 d[\equiv \square]}{dt} = k[\equiv \text{Mn}^{\text{IV}}][\equiv \square - \text{Hg}^0] \\ &= k k_1 [\equiv \text{Mn}^{\text{IV}}][\equiv \square] \end{aligned} \quad (8)$$

So

$$-\frac{d[\equiv \square]}{dt} = k[\equiv \text{Mn}^{\text{IV}}][\equiv \square] \quad (9)$$

$[\equiv \square]$ can be approximately described as:

$$[\equiv \square] = [\equiv \square]_0 \exp(-k[\equiv \text{Mn}^{\text{IV}}]t) \quad (10)$$

Then

$$\frac{d[\equiv \text{Mn}^{\text{II}}\text{Hg}^{\text{II}}]}{dt} = k k_1 [\equiv \text{Mn}^{\text{IV}}][\equiv \square]_0 \exp(-k[\equiv \text{Mn}^{\text{IV}}]t) \quad (11)$$

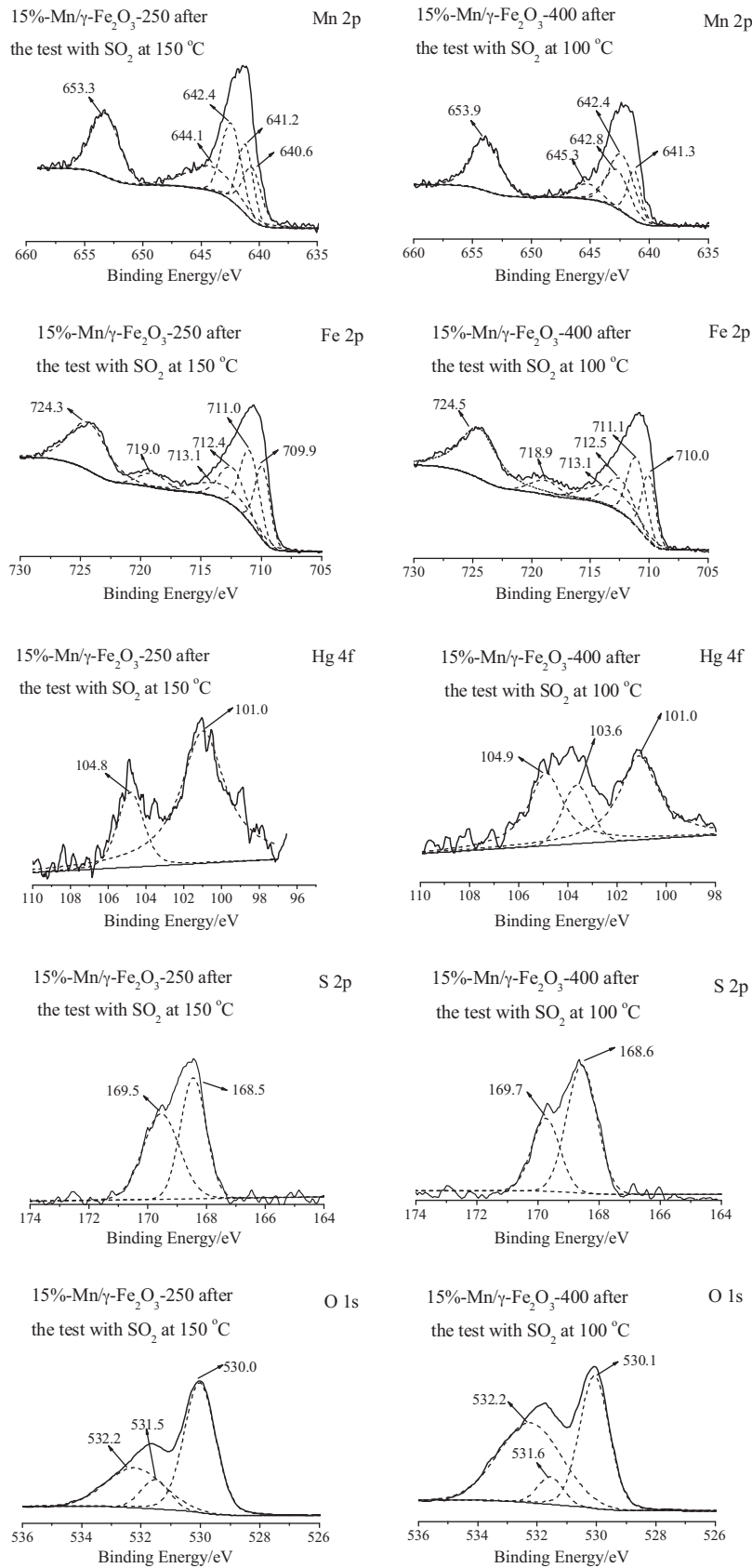


Fig. 5. XPS spectra of synthesized samples after the test with SO₂ over the spectral regions of Mn 2p, Fe 2p, Hg 4f, S 2p and O 1s.

$$[\equiv \text{Mn}^{\text{II}}\text{Hg}^{\text{II}}] = kk_1[\equiv \text{Mn}^{\text{IV}}][\equiv \square]_0 \int_0^t \exp(-k[\equiv \text{Mn}^{\text{IV}}]t) dt \quad (12)$$

So

$$Q = \text{BET} \cdot kk_1[\equiv \text{Mn}^{\text{IV}}][\equiv \square]_0 \int_0^t \exp(-k[\equiv \text{Mn}^{\text{IV}}]t) dt \quad (13)$$

where Q was the amount of elemental mercury captured per unit mass of sorbent, which can be described as the product of BET surface area and the concentration of adsorbed mercury on the surface ($[\equiv \text{Mn}^{\text{II}}\text{Hg}^{\text{II}}]$).

As shown in Eq. (13), the amount of elemental mercury captured should be approximately proportional to the product of BET surface area, $[\equiv \text{Mn}^{\text{IV}}]$ and $[\equiv \square]_0$. But the variation tendency of the capacities of Mn/ γ -Fe₂O₃ for elemental mercury capture did not follow the hypothesis (shown in Table 3).

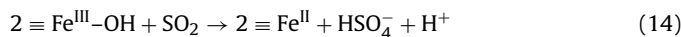
Elemental mercury capture by 30%-Mn/ γ -Fe₂O₃-400 under air at 150 °C was also studied by XPS (shown in Fig. 4). In comparison with fresh 30%-Mn/ γ -Fe₂O₃-400 (shown in Fig. 2), no obvious changes happened over the spectral region of Fe 2p. But the percent of Mn⁴⁺ decreased from 14.0% to 9.9%, and the percent of Mn³⁺ increased from 1.1% to 5.8% (shown in Table 2). Meanwhile, the component corresponding to Mn²⁺ cations did not appear. They suggest that some Mn⁴⁺ cations were only reduced to Mn³⁺ cations. Taking into account the binding energies of Hg 4f 7/2 at 101.0 eV and Hg 4f 5/2 at 105.1 eV, the oxidized mercury formed was still HgO. Therefore, elemental mercury capture by 30%-Mn/ γ -Fe₂O₃-400 may mainly follow Reaction (4). Per unit of Mn⁴⁺ in Reaction (5) can oxidize 1 unit of elemental mercury, but per unit of Mn⁴⁺ in Reaction (4) can only oxidize 0.5 unit of elemental mercury. As a result, the capacities of 15%-Mn/ γ -Fe₂O₃-250 for elemental mercury capture were generally more than those of 30%-Mn/ γ -Fe₂O₃-400, although the percent of Mn⁴⁺ cation on 15%-Mn/ γ -Fe₂O₃-250 was much less than that on 30%-Mn/ γ -Fe₂O₃-400 (shown in Table 2).

The reaction route of elemental mercury oxidization by Mn/ γ -Fe₂O₃ may be dependent on the ratio of $[\equiv \text{Mn}^{4+}]$ to $[\equiv \square - \text{Hg}^0]$. If $[\equiv \text{Mn}^{4+}]/[\equiv \square - \text{Hg}^0]$ was more than 2, elemental mercury capture may mainly follow Reaction (4). If $[\equiv \text{Mn}^{4+}]/[\equiv \square - \text{Hg}^0]$ was less than 1, elemental mercury capture may mainly follow Reaction (5). $[\equiv \text{Mn}^{4+}]/[\equiv \square]$ on 15%-Mn/ γ -Fe₂O₃-250 was 2.2, so $[\equiv \text{Mn}^{4+}]/[\equiv \square - \text{Hg}^0]$ may be close to 1. As a result, elemental mercury capture by 15%-Mn/ γ -Fe₂O₃-250 mainly followed Reaction (5). But $[\equiv \text{Mn}^{4+}]/[\equiv \square]$ on 30%-Mn/ γ -Fe₂O₃-400 was 5.8, so $[\equiv \text{Mn}^{4+}]/[\equiv \square - \text{Hg}^0]$ may be more than 2. As a result, elemental mercury capture by 30%-Mn/ γ -Fe₂O₃-400 may mainly follow Reaction (4). $[\equiv \text{Mn}^{4+}]/[\equiv \square]$ on 15%-Mn/ γ -Fe₂O₃-400 and 30%-Mn/ γ -Fe₂O₃-250 were 2.8 and 3.8, respectively. Elemental mercury capture by 15%-Mn/ γ -Fe₂O₃-400 and 30%-Mn/ γ -Fe₂O₃-250 may mainly follow Reaction (5) at lower temperatures (<150 °C). The constant k_1 rapidly decreased with the increase of reaction temperature, so $[\equiv \text{Mn}^{4+}]/[\equiv \square - \text{Hg}^0]$ obviously increased with the increase of reaction temperature. As a result, elemental mercury capture by 15%-Mn/ γ -Fe₂O₃-400 and 30%-Mn/ γ -Fe₂O₃-250 may follow Reaction (4) at high temperatures (>150 °C). Therefore, elemental mercury capture by Mn/ γ -Fe₂O₃ showed the intricate variation tendency (shown in Table 3).

3.2.2. Effect of SO₂ on elemental mercury capture

The capacities of 15%-Mn/ γ -Fe₂O₃-250 and -400 for elemental mercury capture in the presence of a high concentration of SO₂ (about 2.8 g N m⁻³) are shown in Table 3. The presence of a high concentration of SO₂ resulted in an insignificant effect on elemental mercury capture by 15%-Mn/ γ -Fe₂O₃-250 at lower temperatures (<200 °C). But elemental mercury capture by 15%-Mn/ γ -Fe₂O₃-400 was obviously interfered by the high concentration of SO₂.

Previous research postulated a mechanism for the heterogeneous uptake and oxidization of SO₂ on iron oxides [14]. The overall reaction can be described as:



As shown in Reaction (14), the uptake of SO₂ on iron oxides may involve hydroxyl groups on the surface. Furthermore, SO₂ can also react with Mn⁴⁺ on the surface of MnO₂ [15] and the reaction can be described as:



Elemental mercury capture by 15%-Mn/ γ -Fe₂O₃-250 at 150 °C and it by 15%-Mn/ γ -Fe₂O₃-400 at 100 °C in the presence of a high concentration of SO₂ were studied using XPS analysis (shown in Fig. 5).

The Hg 4f peaks of 15%-Mn/ γ -Fe₂O₃-250 and -400 after the test with SO₂ still centered at about 101 and 105 eV. It indicates that the oxidized mercury formed was still HgO. The S 2p peaks mainly centered at about 168.6 and 169.6 eV, which were assigned to SO₄²⁻ and HSO₄⁻, respectively. The formation of sulfate can also be supported by the XPS spectra over the spectral regions of Fe 2p, Mn 2p and O 1s. The peaks centered at about 713.1, 642.8 and 532.2 eV, may be assigned to Fe 2p 3/2 of Fe₂(SO₄)₃, Mn 2p 3/2 of MnSO₄ and O 1s of SO₄²⁻, respectively. With the formation of sulfate, the percent of $\equiv \text{Fe}^{\text{III}}-\text{OH}$ obviously decreased (shown in Table 2).

The peak centered at about 642.8 eV corresponding to MnSO₄ did not appear in the XPS spectra of 15%-Mn/ γ -Fe₂O₃-250 after the test at 150 °C. The percent of $\equiv \text{Fe}^{\text{III}}-\text{OH}$ was much more than it of Mn⁴⁺ on 15%-Mn/ γ -Fe₂O₃-250, so SO₂ may mainly react with $\equiv \text{Fe}^{\text{III}}-\text{OH}$ and few $\equiv \text{Mn}^{4+}$ reacted with SO₂. As a result, the presence of a high concentration of SO₂ resulted in an insignificant effect on elemental mercury capture by 15%-Mn/ γ -Fe₂O₃-250 at lower temperatures. The amount of $\equiv \text{Fe}^{\text{III}}-\text{OH}$ would decrease due to the dehydroxylation with the increase of reaction temperature, so the high concentration of SO₂ showed an obvious interference with elemental mercury capture by 15%-Mn/ γ -Fe₂O₃-250 at 250–300 °C (shown in Table 3).

The percent of Mn⁴⁺ was almost equal to it of $\equiv \text{Fe}^{\text{III}}-\text{OH}$ on 15%-Mn/ γ -Fe₂O₃-400 (shown in Table 2), so both $\equiv \text{Mn}^{4+}$ and $\equiv \text{Fe}^{\text{III}}-\text{OH}$ reacted with SO₂ even at lower temperatures. As a result, elemental mercury capture by 15%-Mn/ γ -Fe₂O₃-400 was interfered by the high concentration of SO₂. Because 67% of the formed SO₄²⁻ involved $\equiv \text{Fe}^{\text{III}}-\text{OH}$ and only 33% of the formed SO₄²⁻ involved Mn cations, 15%-Mn/ γ -Fe₂O₃-400 still showed an excellent capacity for elemental mercury capture at 100 °C.

4. Conclusion

15%-Mn/ γ -Fe₂O₃-250 showed an excellent capacity for elemental mercury capture, and a high concentration of SO₂ showed an insignificant effect at lower temperatures (100–200 °C). The capacities of 15%-Mn/ γ -Fe₂O₃-250 for elemental mercury capture were more than 2.2 mg g⁻¹ at 100–200 °C in the presence of 2.8 g N m⁻³ of SO₂. Furthermore, the super-paramagnetism made it possible to separate 15%-Mn/ γ -Fe₂O₃-250 from the fly ash. Therefore, 15% Mn/ γ -Fe₂O₃-250 may be a promising sorbent for the control of elemental mercury emission.

In our future work, 15%-Mn/ γ -Fe₂O₃-250 will be investigated to capture elemental mercury from the flue gas at a pilot scale, in which the influence of O₂, SO₂, SO₃, CO, NO_x, HCl, NH₃ and H₂O will be further studied. Furthermore, H₂ will be investigated to regenerate the sorbent. The adsorbed HgO may be reduced to gaseous elemental mercury by H₂ at 250 °C. The concentration of elemental mercury in the exhaust of the regeneration may be much higher than that in the flue gas, so it may be collected as liquid mercury

at room temperature for safe disposal. 15% Mn/ γ -Fe₂O₃-250 may be reduced by H₂ during the regeneration. But it may be recovered after the thermal treatment at 250 °C under air.

Acknowledgements

This study was supported by the High-Tech R&D Program of China (no. 2007AA06Z340) and Shanghai Tongji Gao Tingyao Environmental Science & Technology Development Foundation.

References

- [1] W.J. Lee, G.N. Bae, Removal of elemental mercury (Hg(O)) by nanosized V₂O₅/TiO₂ catalysts, *Environ. Sci. Technol.* 43 (2009) 1522–1527.
- [2] A.A. Presto, E.J. Granite, Survey of catalysts for oxidation of mercury in flue gas, *Environ. Sci. Technol.* 40 (2006) 5601–5609.
- [3] D.G. Streets, J.M. Hao, Y. Wu, J.K. Jiang, M. Chan, H.Z. Tian, X.B. Feng, Anthropogenic mercury emissions in China, *Atmos. Environ.* 39 (2005) 7789–7806.
- [4] N.Q. Yan, Z. Qu, Y. Chi, S.H. Qiao, R.L. Dod, S.G. Chang, C. Miller, Enhanced elemental mercury removal from coal-fired flue gas by sulfur–chlorine compounds, *Environ. Sci. Technol.* 43 (2009) 5410–5415.
- [5] C.E. Romero, Y. Li, H. Bilirgen, N. Sarunac, E.K. Levy, Modification of boiler operating conditions for mercury emissions reductions in coal-fired utility boilers, *Fuel* 85 (2006) 204–212.
- [6] L. Ji, P.M. Sreekanth, P.G. Smirniotis, S.W. Thiel, N.G. Pinto, Manganese oxide/titania materials for removal of NO_x and elemental mercury from flue gas, *Energy Fuels* 22 (2008) 2299–2306.
- [7] D.Y. Lu, D.L. Granatstein, D.J. Rose, Study of mercury speciation from simulated coal gasification, *Ind. Eng. Chem. Res.* 43 (2004) 5400–5404.
- [8] S.X. Wang, L. Zhang, G.H. Li, Y. Wu, J.M. Hao, N. Pirrone, F. Sprovieri, M.P. Ancora, Mercury emission and speciation of coal-fired power plants in China, *Atmos. Chem. Phys.* 10 (2010) 1183–1192.
- [9] J. Dong, Z.H. Xu, S.M. Kuznicki, Magnetic multi-functional nano composites for environmental applications, *Adv. Funct. Mater.* 19 (2009) 1268–1275.
- [10] H.Q. Yang, Z.H. Xu, M.H. Fan, A.E. Bland, R.R. Judkins, Adsorbents for capturing mercury in coal-fired boiler flue gas, *J. Hazard. Mater.* 146 (2007) 1–11.
- [11] Y. Liu, Z.H. Xu, S.M. Kuznicki, Development of a novel mercury cartridge for mercury analysis, *Energy Fuels* 24 (2010) 10–17.
- [12] A.A. Presto, E.J. Granite, Impact of sulfur oxides on mercury capture by activated carbon, *Environ. Sci. Technol.* 41 (2007) 6579–6584.
- [13] A.A. Presto, E.J. Granite, A. Karash, Further investigation of the impact of sulfur oxides on mercury capture by activated carbon, *Ind. Eng. Chem. Res.* 46 (2007) 8273–8276.
- [14] H.B. Fu, X. Wang, H.B. Wu, Y. Yin, J.M. Chen, Heterogeneous uptake and oxidation of SO₂ on iron oxides, *J. Phys. Chem. C* 111 (2007) 6077–6085.
- [15] W.S. Kijlstra, M. Biervliet, E.K. Poels, A. Blik, Deactivation by SO₂ of MnO_x/Al₂O₃ catalysts used for the selective catalytic reduction of NO with NH₃ at low temperatures, *Appl. Catal. B: Environ.* 16 (1998) 327–337.
- [16] S. Yang, Y. Guo, N. Yan, D. Wu, H. He, J. Xie, Z. Qu, C. Yang, J. Jia, A novel multi-functional magnetic Fe–Ti–V spinel catalyst for elemental mercury capture and callback from flue gas, *Chem. Commun.* 46 (2010) 8377–8379.
- [17] S. Yang, Y. Guo, N. Yan, D. Wu, H. He, J. Xie, Z. Qu, J. Jia, Remarkable effect of the incorporation of titanium on the catalytic activity and SO₂ poisoning resistance of magnetic Mn–Fe spinel for elemental mercury capture, *Appl. Catal. B: Environ.*, (2010), doi:10.1016/j.apcatb.2010.11.012.
- [18] J. Dong, Z.H. Xu, S.M. Kuznicki, Mercury removal from flue gases by novel regenerable magnetic nanocomposite sorbents, *Environ. Sci. Technol.* 43 (2009) 3266–3271.
- [19] E.J. Granite, H.W. Pennline, R.A. Hargis, Novel sorbents for mercury removal from flue gas, *Ind. Eng. Chem. Res.* 39 (2000) 1020–1029.
- [20] J.F. Li, N.Q. Yan, Z. Qu, S.H. Qiao, S.J. Yang, Y.F. Guo, P. Liu, J.P. Jia, Catalytic oxidation of elemental mercury over the modified catalyst Mn/ α -Al₂O₃ at lower temperatures, *Environ. Sci. Technol.* 44 (2010) 426–431.
- [21] S. Yang, H. He, D. Wu, D. Chen, X. Liang, Z. Qin, M. Fan, J. Zhu, P. Yuan, Decolorization of methylene blue by heterogeneous Fenton reaction using Fe_{3–x}Ti_xO₄ (0 ≤ x ≤ 0.78) at neutral pH values, *Appl. Catal. B: Environ.* 89 (2009) 527–535.
- [22] Y. Zhang, M. Yang, X.M. Dou, H. He, D.S. Wang, Arsenate adsorption on an Fe–Ce bimetal oxide adsorbent: role of surface properties, *Environ. Sci. Technol.* 39 (2005) 7246–7253.
- [23] T. Herranz, S. Rojas, M. Ojeda, F.J. Perez-Alonso, P. Tefferos, K. Pirola, J.L.G. Fierro, Synthesis, structural features, and reactivity of Fe–Mn mixed oxides prepared by microemulsion, *Chem. Mater.* 18 (2006) 2364–2375.
- [24] R.M. Cornell, U. Schwertmann, *The Iron Oxides: Structure, Properties, Reactions Occurrences and Uses*, 2nd ed., Wiley-VCH, New York, 2003.